Editors' Choice

ORIGINAL PAPER

Evaluation of system-related magnetic resonance imaging geometric distortion in radiation therapy treatment planning: two approaches and effectiveness of three-dimensional distortion correction

Yutaka Kato[1], Kuniyasu Okudaira[1], Takeshi Kamomae[2], Motoki Kumagai[2],
Youta Nagai[1], Toshiaki Taoka[2], Yoshiyuki Itoh[2] and Shinji Naganawa[2]

[1]*Department of Radiological Technology, Nagoya University Hospital, Nagoya, Japan*
[2]*Department of Radiology, Nagoya University Graduate School of Medicine, Nagoya, Japan*

ABSTRACT

We propose two methods to evaluate system-related distortion in magnetic resonance imaging (MRI) in radiation therapy treatment planning (RTP) and demonstrate the importance of three-dimensional (3D) distortion correction (DC) by quantitatively measuring the distortion magnitude. First, a small pin phantom was scanned at multiple positions using an external laser guide for accurate phantom placement and combined into one image encompassing a large area. Direct plane images were used for evaluating in-plane distortion and multiplanar reconstruction images for through-plane distortion with no DC, two-dimensional (2D) DC, and 3D DC. Second, a large grid sheet was scanned as the direct plane of the phantom placement. The distortion magnitude was determined by measuring the displacement between the MRI and reference coordinates. The measured distortions were compared between in- and through-plane when applying DC and between the two methods. The small pin phantom method can be used to evaluate a wide range of distortions, whereas data from the entire plane can be obtained with a single scan using the grid sheet without a laser guide. The mean distortion magnitudes differed between the methods. Furthermore, the 3D DC reduced in- and through-plane distortions. In conclusion, the small pin phantom method can be used to evaluate a wide range of distortions by creating a combined image, whereas the grid sheet method is simpler, accurate, repeatable, and does not require a special-order phantom or laser guide. As 3D DC reduces both in- and through-plane distortions, it can be used to improve RTP quality.

Keywords: distortion, magnetic resonance imaging, radiation therapy treatment planning, system-related distortion, distortion correction

Abbreviations:
MRI: magnetic resonance imaging
RTP: radiation therapy treatment planning
CT: computed tomography
2D: two-dimensional
3D: three-dimensional
DC: distortion correction
FOV: field-of-view

CP: control point

INTRODUCTION

The use of magnetic resonance imaging (MRI) in radiation therapy treatment planning (RTP) is increasing because of its superior soft-tissue contrast compared with that of computed tomography (CT), and high spatial resolution comparable with that of CT afforded by recent technological advances.[1-3] In addition, radiation therapy can now yield more localized and customized irradiation that maximizes the dose delivered to tumors while sparing adjacent healthy tissue (eg, intensity-modulated radiation therapy or stereotactic radiation therapy). In RTP, precise geometric information regarding the shape and location of the tumors and surrounding healthy tissues must be obtained. Hence, more accurate spatial information is required for more precise targeting.

A dedicated system is preferred for MRI in RTP (Fig. 1) to achieve an examination environment different from that of diagnostic MRI. First, the patient must be placed in a position identical to that used in radiation treatment. However, MRI beds are not necessarily compatible with radiation treatment units because most MRI beds are concave with soft padding for ensuring patient comfort over a long time period. Therefore, a rigid flat couch must be placed over the standard receiver coil. In addition, the anterior receiver coil must not be in direct contact with the patient to avoid changing their body surface shape. These measures increase the distance from the receiver coil to the patient.[4,5] Second, it is crucial to conduct the scan while fixing the

Fig. 1 Dedicated 3T MRI scanner (MAGNETOM Skyra, Siemens, Erlangen, Germany) with an external laser control system (DORADOnova MR3T LAP GmbH Laser Applikationen, Luneburg, Germany) and flat table overlay (Civco Medical Instruments Inc.) placed over a standard receiver coil

patient's position using a thermoplastic mask (ie, a shell). This ensures the reproducibility of the patient's position; accordingly, the optimal receiver coil used in diagnostic examinations is not applicable for MRI in RTP.[6-8] If either of these conditions is satisfied, then the signal-to-noise ratio will be decreased. Therefore, adapting MRI examinations based on treatment position may compromise image quality. Nevertheless, because precise target contouring requires higher spatial resolution and thinner slices compared with diagnostic examinations, a 3T scanner is preferred to achieve adequate signal-to-noise ratio.

However, the major limitation regarding the use of MRI in RTP has been identified as the deterioration in spatial accuracy caused by distortion. The 3T scanner is generally associated with large distortions caused by several factors,[9] and geometric distortions are further enhanced in modern scanners that use a shorter bore magnet and a faster and stronger gradient system. MRI is typically affected by system- and patient-related distortions that alter the accurate representation of anatomical structures. System-related distortions are generated by static magnetic field (B_0) inhomogeneity and gradient nonlinearity that are inherent to the scanner. In contrast, patient-related distortions are caused by magnetic susceptibility and chemical shift.[10,11] Furthermore, the gradient nonlinearity is sequence independent, whereas the others (B_0 inhomogeneity, magnetic susceptibility, and chemical shift) are sequence dependent.[10] Although minor distortions in MRI generally result in few consequences on routine clinical examination results, geometric distortions can be a serious problem in RTP for cases that require high geometric accuracy, and the unavoidable distortion can affect the anatomical coordinate system, thereby undermining the quality of the implemented RTP.[12] Therefore, magnetic resonance images must be corrected to reduce distortions to a degree that can be tolerated in RTP (eg, a spatial accuracy of up to 2 mm is required for radiation therapy[13]), or the tolerated area for each sequence and scanner must be determined.

A considerable number of published studies have addressed the mechanism of distortion and offered methods that can be used to correct the resulting artifacts.[14-20] Two reports have comprehensively summarized the effects of distortion in MRI for radiation therapy.[10,11] Additionally, previous studies have provided detailed characterizations of geometric distortion and reported the performance of vendor-specific two-dimensional (2D) and three-dimensional (3D) geometric distortion correction (DC) over a large field-of-view (FOV).[21,22] However, as these studies used special-order, large, dedicated phantoms that are not currently available commercially, the results are difficult to reproduce in many facilities. The aim of the present study were as follows: (1) to propose two methods for evaluating system-related geometric distortions over a large FOV without using special dedicated phantoms, (2) to quantitatively evaluate geometric distortions using vendor-specific DC, and (3) to demonstrate the importance of 3D DC application in RTP.

MATERIALS AND METHODS

Phantom scans were performed on a 3T scanner (MAGNETOM Skyra, Siemens, Erlangen, Germany) using a body coil. Images were obtained based on the following three sequences: 2D T_2-weighted fast spin-echo, 3D T_2-weighted fast spin-echo, and 3D T_1-weighted gradient echo. The scan parameters used for the sequences are summarized in Table 1.

Table 1 Pulse sequences and parameters

| Parameter	2D T$_2$-weighted	3D T$_2$-weighted	3D T$_1$-weighted
Type	Fast spin echo	Fast spin echo	Gradient echo
Repetition time (ms)	6000	2500	1570
Echo time (ms)	98	340	2.29
Flip angle (degree)	90/150	Variable	15
Field-of-view (mm)	500	500	500
Matrix size	512 × 512	512 × 512	512 × 512
Spatial resolution (mm)	0.98 × 0.98 × 2.0	0.98 × 0.98 × 1.0	0.98 × 0.98 × 1.0
Band width (Hz/Pixel)	200	698	200

2D: two-dimensional
3D: three-dimensional

Small Pin Phantom Method

For the first attempt, we used a 220-mm-diameter phantom (90–401 type; Nikko Fines Industries Co., Ltd., Tokyo, Japan), with 10-mm-diameter pins placed at 20-mm intervals (Fig. 2a). These pins are made of acrylic, and the surrounding area is filled with polyvinyl alcohol components. This is a well-known phantom used in various performance evaluations and has already been established at many domestic institutions. As the phantom cannot acquire an image encompassing a large area in a single scan, the phantom was scanned at multiple positions with an 80-mm overlap (eg, three different positions along the *x*-axis by three different positions along the *z*-axis in the coronal phantom placement; Fig. 3) to encompass the maximum 500-mm FOV of the scanner. To evaluate the three axes, coronal, sagittal, and axial scans were performed in each of the phantom placements parallel to the x-z, y-z, and x-y planes, using identical FOV settings. For accurate alignment of the phantom, we used a well-calibrated 3D external laser control system (DORADOnova MR3T LAP GmbH Laser Applikationen, Luneburg, Germany). Images of multiple positions were further combined on the scanner console into a single large image that encompassed a wide range of FOVs. In the orthogonal plane of the phantom placement, multiplanar reconstruction was performed and then combined. Direct plane images were used for evaluating in-plane distortions (eg, coronal scan for coronal phantom placement), and multiplanar reconstruction images were used for evaluating through-plane distortions (eg, sagittal and axial scans for coronal phantom placement). All images were reconstructed without DC, and vendor-specific 2D and 3D DCs were applied by retrospective reconstruction. The spatial coordinates of each pin, which were calculated theoretically from the nominal design specifications, were adopted as the reference coordinates (RCs).

Grid Sheet Phantom Method

To facilitate the procedure, a larger phantom was prepared using a polystyrene resin grid sheet (LGP-15-11, HOSEI Co., Ltd., Osaka, Japan) to encompass a large FOV with a single scan. The external dimensions were 380 × 380 mm, the distance between the grid intersections was 15 mm, and the cell size was 14.5 × 14.5 × 11.0 mm (Fig. 2b). The sheet contained 27 grid crosses along the vertical and horizontal axes, producing 729 measurement points. Such sheets are typically used for building ventilation and can be purchased commercially. To compare the small pin phantom method with the in-plane distortion, the grid sheet was placed parallel to each plane in a water tank (400 × 400 × 400 mm), and the surrounding area was filled with the minimum

amount of tap water required to avoid radio-frequency field (B_1) inhomogeneity.[23] Because the copper sulfate solution used in most MRI-phantoms is costly, and owing to domestic regulations on drainage, we used tap water, which is the easiest to prepare and replace. Each direct plane image was obtained for the three sequences, both with and without DC. Subsequently, the RC of the grid sheet was acquired using a CT scanner (SOMATOM Confidence RT Pro, Siemens, Erlangen, Germany) because construction errors might occur when using the nominal design specifications of the sheet. The voxel size of the CT data set was $1.07 \times 1.07 \times 1.00$ mm.
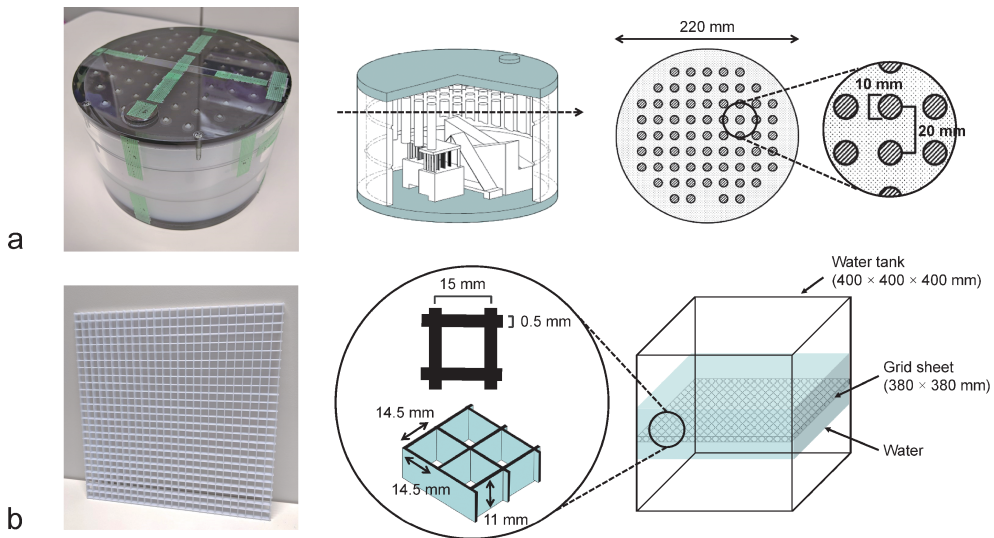
Fig. 2   Photographs of phantoms and schematic illustrations
Fig. 2a: Pin phantom.
Fig. 2b: Grid sheet phantom.
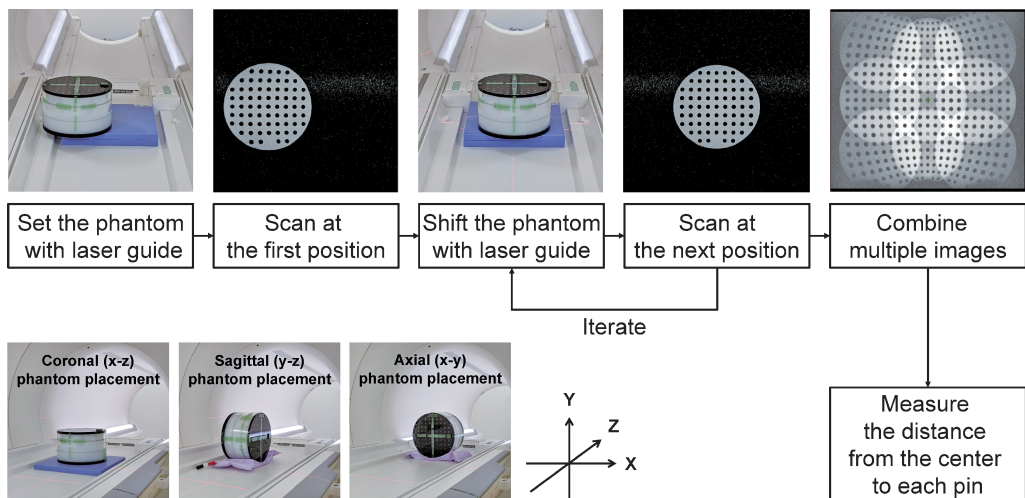
**Fig. 3**   Flowchart of the small pin phantom method

Image Analysis

To quantitatively determine the amount of distortion, the coordinates as a control point (CP) were determined using an in-house MATLAB program (MathWorks, Inc., Natick, MA, USA). The first step was to derive binary images using thresholds and identify the CPs using a cross-filter. The next step was to determine the final coordinates by visually inspecting and manually modifying all CPs. The analysis excluded some CPs that could not be detected automatically because of severe distortion or signal loss. Furthermore, the distance from the magnetic isocenter to each CP was measured, and the measured distributions were compared with the location of the corresponding RC data. The distortion was calculated using the following formula:

$$Distortion = \sqrt{(X_{MRI} - X_{RC})^2 + (Y_{MRI} - Y_{RC})^2 + (Z_{MRI} - Z_{RC})^2}$$

The final geometric distortion was calculated as the mean distortion magnitude within the identical area at 20-mm intervals from the magnetic isocenter up to 240 mm. The measured distortions were evaluated for differences between the following: (1) the in- and through-planes when applying DC, (2) both evaluation methods, and (3) sequences.

RESULTS

Figure 4 shows the representative combined images obtained from multiple positions of the coronal phantom placement using the small pin phantom method with no DC, 2D DC, and 3D DC. The combined image from the pin phantom theoretically yielded a maximum of 422 CPs on the entire plane. Both directions (*x*- and *z*-axes) in the upper row exhibited in-plane distortions, whereas the slice direction (*z*-axis) in the lower row exhibited through-plane distortions. Different degrees of distortion were identified among the DC types. Although the 2D and 3D DC performances did not differ in terms of in-plane distortions, a significant difference was observed in terms of through-plane distortions. Figure 5 shows the representative direct plane images of the coronal phantom placement using the grid sheet method with no DC, 2D DC, and the corresponding CT image. Although the small pin phantom method required multiple scans, we were able to obtain an entire plane image in a single scan using the grid sheet method. Figure 6 shows the changes in mean distortion magnitude with distance from the magnetic isocenter in three sequences for both in- and through-plane distortions using the small pin phantom method. The mean distortion magnitude increased with increasing distance from the magnetic isocenter, except at a distance of 240 mm. The 3D DC reduced in-plane and through-plane distortions. Figure 7 shows comparison of the two methods with and without DC for the mean in-plane distortion magnitudes. The mean distortion magnitudes obtained via the two methods were inconsistent, particularly around the edge of the FOV. The maximums, means, and standard deviations of the distortion magnitudes when applying DC in the grid sheet phantom method are summarized in Table 2. Figure 8 shows a comparison of the different sequences when applying DC for the mean distortion magnitudes. In all cases, we found that distortion varied depending on the sequence.
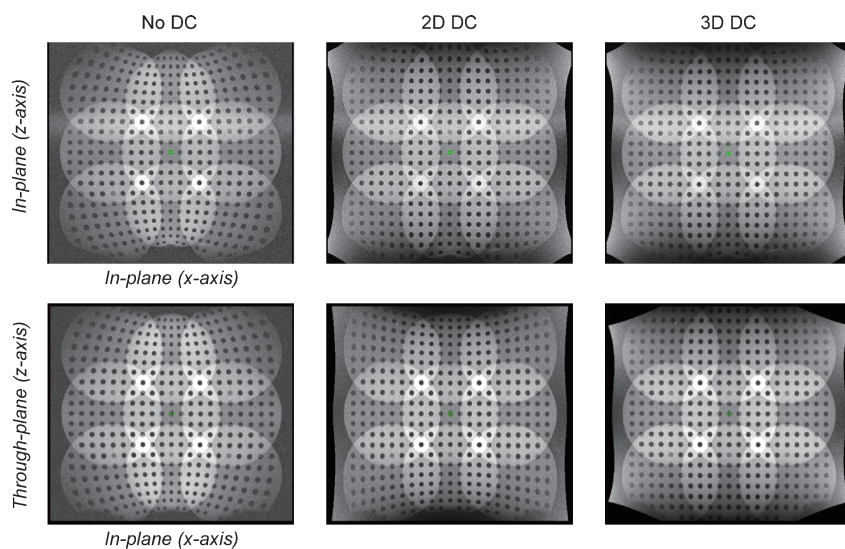
Fig. 4 Representative combined images of multiple positions of coronal phantom placement using the small pin phantom method with no DC, 2D DC, and 3D DC
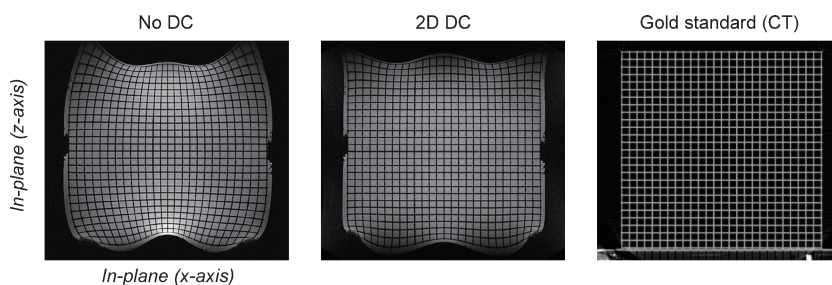
Upper row: Direct coronal plane of axial images.

Lower row: Multiplanar reconstructed coronal plane of axial images.

2D: two-dimensional

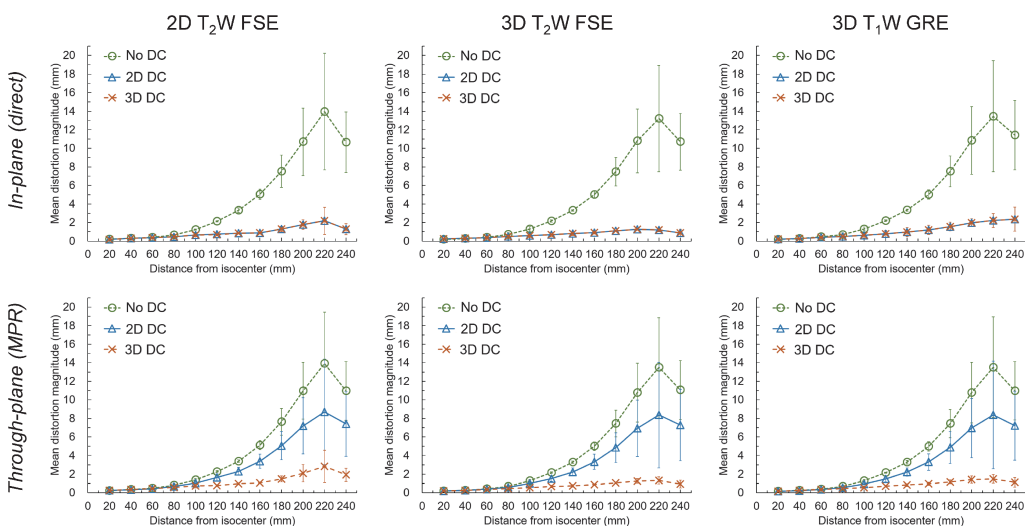3D: three-dimensional

DC: distortion correction

Fig. 5 Representative direct plane images of coronal phantom placement using the grid sheet method with no DC, 2D DC, and the corresponding CT image
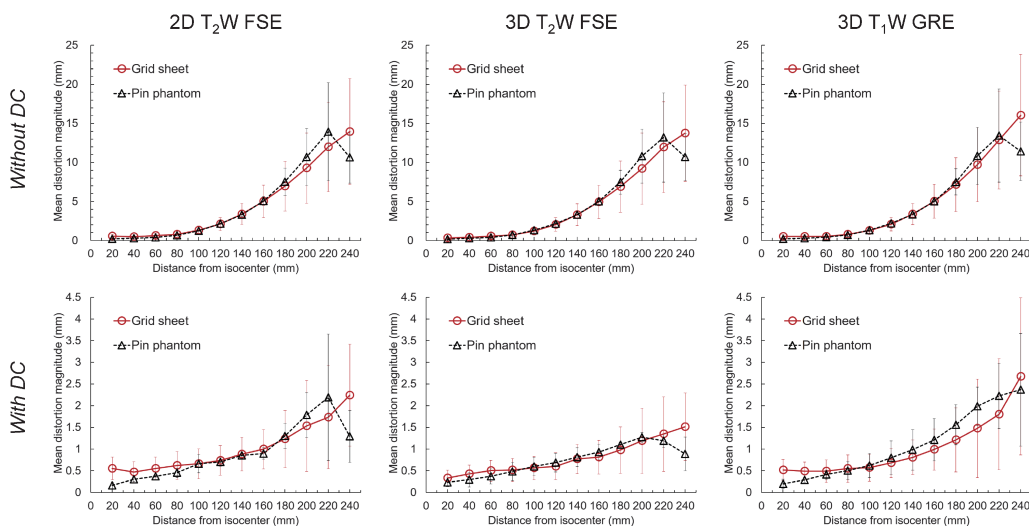
DC: distortion correction

2D: two-dimensional

CT: computed tomography

Fig. 6 Mean distortion magnitudes obtained using the small pin phantom method for three sequences in
in-plane (upper) and through-plane (lower)

2D: two-dimensional
3D: three-dimensional
T_2W: T_2-weighted
T_1W: T_1-weighted
FSE: fast spin-echo
GRE: gradient echo
DC: distortion correction

Fig. 7 Comparisons of in-plane mean distortion magnitudes between the two methods without (upper) and
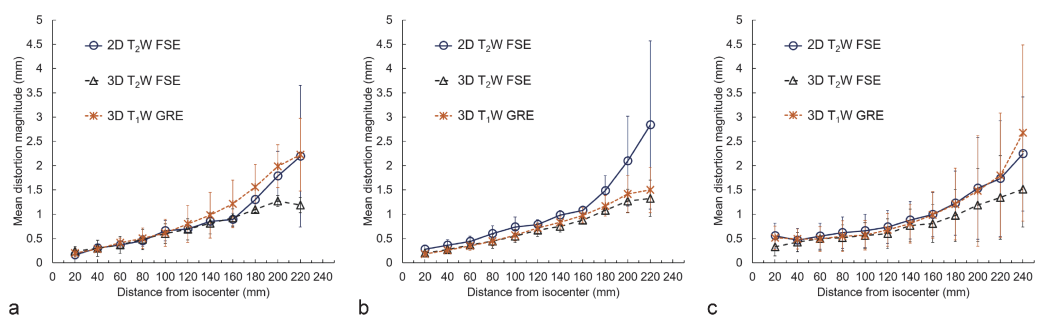with (lower) DC

2D: two-dimensional
3D: three-dimensional
T_2W: T_2-weighted
T_1W: T_1-weighted
FSE: fast spin-echo
GRE: gradient echo
DC: distortion correction

Fig. 8 Comparisons of mean distortion magnitudes between different sequences with distortion correction applied

Fig. 8a: In-plane for pin phantom.
Fig. 8b: Through-plane for pin phantom.
Fig. 8c: In-plane for grid sheet phantom.
2D: two-dimensional
3D: three-dimensional
T₂W: T₂-weighted
T₁W: T₁-weighted
FSE: fast spin-echo
GRE: gradient echo

Table 2 Distortion magnitudes when applying distortion correction using the grid sheet phantom method

Distance from isocenter (mm)	2D T₂-weighted FSE		3D T₂-weighted FSE		3D T₁-weighted GRE	
	Mean ± SD (mm)	Maximum (mm)	Mean ± SD (mm)	Maximum (mm)	Mean ± SD (mm)	Maximum (mm)
0–20	0.55 ± 0.26	0.98	0.33 ± 0.18	0.72	0.52 ± 0.24	0.97
20–40	0.47 ± 0.23	0.90	0.43 ± 0.20	0.88	0.49 ± 0.21	1.11
40–60	0.55 ± 0.27	1.47	0.50 ± 0.24	1.05	0.49 ± 0.26	1.18
60–80	0.62 ± 0.32	1.39	0.52 ± 0.27	1.24	0.55 ± 0.31	1.35
80–100	0.66 ± 0.34	1.82	0.56 ± 0.27	1.21	0.57 ± 0.31	1.39
100–120	0.74 ± 0.34	1.65	0.60 ± 0.31	1.64	0.68 ± 0.33	1.66
120–140	0.88 ± 0.39	2.09	0.77 ± 0.34	1.87	0.81 ± 0.40	1.93
140–160	0.99 ± 0.45	2.08	0.81 ± 0.39	2.24	0.99 ± 0.48	2.65
160–180	1.23 ± 0.66	3.75	0.97 ± 0.54	2.75	1.21 ± 0.74	4.24
180–200	1.53 ± 1.05	5.89	1.19 ± 0.75	3.77	1.48 ± 1.14	6.23
200–220	1.73 ± 1.19	5.93	1.34 ± 0.86	4.34	1.80 ± 1.28	6.71
220–240	2.24 ± 1.17	5.45	1.51 ± 0.78	3.55	2.67 ± 1.81	7.15

2D: two-dimensional
3D: three-dimensional
FSE: fast spin-echo
GRE: gradient-echo
SD: standard deviation

DISCUSSION

For a complete mapping of the geometric distortion in MRI, it is ideal to define the CP in three dimensions. However, in most previous reports,[14-19,22] the 3D phantoms used for encompassing a large volume are heavy, cumbersome, and not acquirable because of their special production requirements. Therefore, to encompass a large FOV, we proposed two methods in this study: (1) an existing phantom (albeit small), and (2) a phantom that can be easily prepared using commercially available materials. In addition, the geometric distortion was evaluated quantitatively by applying a vendor-specific DC. The use of 3D DC significantly improved the geometric accuracy; furthermore, using the grid sheet method, we showed that geometric distortion can be measured in a simple, time-efficient, and cost-efficient manner.

Despite using 2D phantoms in this study, we were able to evaluate the in-plane distortion by directly imaging along the plane of the phantom placement, whereas through-plane distortions could be evaluated by multiplanar reconstruction imaging from the orthogonal plane scan of the phantom placement. Using the small pin phantom method, the combined image could be used to evaluate a wide range of distortions, despite the small phantom size. Although applying the existing phantom was advantageous, scanning had to be performed several times with the phantom positioned at different locations to obtain all data in the entire plane in a large FOV; this process was time consuming. Additional errors can be easily introduced during the repositioning process. In the present study, the problem of misalignment was resolved using an external laser guide. However, not all MRI systems for radiation therapy provide an external laser guide. In contrast, the grid sheet phantom method can be used to obtain the data of an entire plane at once, rendering the process more time-efficient. Moreover, the non-requirement for an external laser guide is advantageous as it allows the method to be applied to any scanner. Conversely, preparing the phantom before performing the scan is a labor-intensive process; it requires the removal of air bubbles that can introduce artifacts,[18] a wait of approximately 30 min before scanning to allow the water to settle, or an adjustment of the minimum required amount of water to maintain a homogeneous radio-frequency pulse while mitigating the standing wave effect.[23] Although costly, the use of copper sulfate solutions to fill the area around the grid sheet can mitigate B_1 inhomogeneity.

In the quantitative measurements, the system-related geometric distortion varied according to the distance from the magnetic isocenter, measurement method, and sequence. In the small pin phantom method, although the mean distortion magnitude decreased at the 240-mm position (Fig. 6), this was considered to be an error attributable to fewer CPs because some CPs at the edge of the FOV could not be identified because of signal loss due to severe distortion. The 3D DC significantly improved spatial accuracy not only in the in-plane, but also in the through-plane direction, which means that 3D DCs are indispensable for correcting 3D volume spatial distortions. In addition, the degree of distortion depended on the sequence in the presence of DC (Fig. 8). A previous study showed that the distortion magnitude and patterns varied among MRI sequence protocols and scanners.[19] In the present study, the fewer distortions observed in the 3D T_2-weighted fast spin-echo image might be attributed to a high bandwidth,[9] whereas the significant distortions of the 2D T_2-weighted fast spin-echo images for the through-plane (Fig. 8b) might be due to poor resolution in the slice directions, where slice thickness was 2 mm. For treatment planning, although 3D DCs should be applied, utilizing DC algorithms does not completely remove distortions. A previous study showed that spatial disposition can significantly affect treatment planning.[24] The authors demonstrated that spatial accuracy should be less than 1.5 mm (target: >20 mm) and less than 1.0 mm (target: ≤20 mm). It is essential to determine the distance from the magnetic isocenter to ensure the accuracy of RTP in each sequence and

the scanner used in RTP. Even when imaging a relatively small volume, patients are not always centered on the magnetic isocenter and shifts of a few centimeters can easily occur, or the RTP target may not always be at the center of the patient. Therefore, a larger volume should be mapped accurately to provide sufficient geometric information.

We identified differences in the mean distortion magnitude between the two methods, particularly around the edge of the FOV (Fig. 7). These differences might have been caused by the properties of the CPs that were also related to the abovementioned CP identification error. A previous study demonstrated that the evaluation accuracy increased with increasing numbers of measurement points.[10] In the present study, although some CPs could not be measured, the combined image using the small pin phantom method yielded a maximum of 422 CPs on the entire plane, whereas the grid sheet comprised 729 CPs. The spacing of the measurement points was 20 and 15 mm for the pin phantom and grid sheet methods, respectively. Because finer measurement points resulted in higher accuracy, the number of CPs must be sufficiently large to understand the accurate spatial variation of distortion in a large FOV. In addition, in the small pin phantom method, the theoretical coordinates were adopted from the nominal design specifications, which may have some construction errors. Therefore, in the grid sheet method, the RC was obtained from the corresponding CT data, which may have been the result of different distortion magnitudes between the two methods. Within the range of <1 mm, differences in the distortion magnitudes were errors because the in-plane resolution (0.98×0.98 mm) could be regarded as the lower measurement limit. Based on these considerations, it can be concluded that the grid sheet method provides more accurate geometric information. Therefore, because the grid sheet method without an external laser guide is both cost and time-efficient and provides good accuracy, it can be used for multiple measurements, such as for assessment of reproducibility and comparisons between sequences or scanners.

Our study has a few limitations. First, this study focused on system-related distortions. However, we did not eliminate object-induced distortions (ie, magnetic susceptibility of the phantom material) because the magnetic susceptibility-induced distortions had a smaller magnitude than the system-related distortions.[10] If necessary, the reversed read gradient polarity technique[17,25] can be used to exclude susceptibility-induced effects. In addition, the total geometric distortion in clinical examinations is imaged as the sum of system- and patient-related distortion. Patient-related distortions typically occur because of magnetic susceptibility and chemical shift effects due to complex anatomical structures, such as the presence of air cavities.[10] Because these artifacts are not negligible in 3T scanners and depend on the sequence parameter, it may be ideal to perform evaluations with the phantom mimicking the patient's shape and anatomical location, such as those developed by Kamomae et al[26] to obtain more accurate RTP in each patient. Recently, ultrashort echo time sequence has been proposed[27] to visualize previously invisible tissues with very short T_2, such as cortical bone, tendons, and ligaments. This sequence has been increasingly used in MRI-only simulation because of its ability to reduce susceptibility artifacts and allow conversions from MRI voxel intensities to Hounsfield units.[28,29] Future research is required to evaluate the geometric distortion using the ultrashort echo time sequence. Second, full 3D volume data were not analyzed because we measured the CPs only in the plane of the three directions. However, our results provided sufficient information regarding the difference in DC performance between in- and through-plane distortions, demonstrating the effectiveness of 3D DCs in MRI for RTP. If necessary, full 3D volume data can be obtained by stacking multiple grid sheets without purchasing a special-order dedicated phantom.

CONCLUSION

We proposed two quantitative methods for evaluating system-related geometric distortions. Using the small pin phantom method, a wide range of distortions was evaluated by creating a combined image from multiple scans. We revealed that the grid sheet phantom method is a simpler, more accurate, and repeatable method that does not require a special-order phantom or any external laser guide. As 3D DC reduced both in- and through-plane distortions, it can be used to improve the quality of RTP.

AUTHOR CONTRIBUTIONS

YK and KO contributed equally to this work.

DISCLOSURE STATEMENT

The authors declare that they have no conflict of interest.

ETHICAL APPROVAL

This article does not contain any studies with human participants or animals performed.

REFERENCES

1 Khoo VS, Dearnaley DP, Finnigan DJ, Padhani A, Tanner SF, Leach MO. Magnetic resonance imaging (MRI): considerations and applications in radiotherapy treatment planning. *Radiother Oncol*. 1997;42(1):1–15. doi:10.1016/s0167-8140(96)01866-x.

2 Rasch C, Barillot I, Remeijer P, Touw A, van Herk M, Lebesque JV. Definition of the prostate in CT and MRI: a multi-observer study. *Int J Radiat Oncol Biol Phys*. 1999;43(1):57–66. doi:10.1016/s0360-3016(98)00351-4.

3 Prabhakar R, Haresh KP, Ganesh T, Joshi RC, Julka PK, Rath GK. Comparison of computed tomography and magnetic resonance based target volume in brain tumors. *J Cancer Res Ther*. 2007;3(2):121–123. doi:10.4103/0973-1482.34694.

4 Kapanen M, Collan J, Beule A, Seppälä T, Saarilahti K, Tenhunen M. Commissioning of MRI-only based treatment planning procedure for external beam radiotherapy of prostate. *Magn Reson Med*. 2013;70(1):127–135. doi:10.1002/mrm.24459.

5 Liney GP, Moerland MA. Magnetic resonance imaging acquisition techniques for radiotherapy planning. *Semin Radiat Oncol*. 2014;24(3):160–168. doi:10.1016/j.semradonc.2014.02.014.

6 Hanvey S, Glegg M, Foster J. Magnetic resonance imaging for radiotherapy planning of brain cancer patients using immobilization and surface coils. *Phys Med Biol*. 2009;54(18):5381–5394. doi:10.1088/0031-9155/54/18/002.

7 Hanvey S, McJury M, Tho LM, et al. The influence of MRI scan position on patients with oropharyngeal cancer undergoing radical radiotherapy. *Rad Oncol*. 2013;28(8):129. doi:10.1186/1748-717X-8-129

8 Paulson ES, Erickson B, Schultz C, Allen Li X. Comprehensive MRI simulation methodology using a dedicated MRI scanner in radiation oncology for external beam radiation treatment planning. *Med Phys*. 2015;42(1):28–39. doi:10.1118/1.4896096.

9 Dietrich O, Reiser MF, Schoenberg SO. Artifacts in 3-T MRI: physical background and reduction strategies. *Eur J Radiol*. 2008;65(1):29–35. doi:10.1016/j.ejrad.2007.11.005.

10 Weygand J, Fuller CD, Ibbott GS, et al. Spatial precision in magnetic resonance imaging-guided radiation therapy: the role of geometric distortion. *Int J Radiat Oncol Biol*. Phys 2016;95(4):1304–1316. doi:10.1016/j.ijrobp.2016.02.059.

11   Schmidt MA, Payne GS. Radiotherapy planning using MRI. *Phys Med Biol*. 2015;60(22):R323–R361. doi:10.1088/0031-9155/60/22/R323.

12   Seibert TM, White NS, Kim GY, et al. Distortion inherent to magnetic resonance imaging can lead to geometric miss in radiosurgery planning. *Pract Radiat Oncol*. 2016;6(6):e319–e328. doi:10.1016/j.prro.2016.05.008.

13   Kutcher GJ, Coia L, Gillin M, et al. Comprehensive QA for radiation oncology: report of AAPM Radiation Therapy Committee Task Group 40. *Med Phys*. 1994;21(4):581–618. doi:10.1118/1.597316.

14   Mizowaki T, Nagata Y, Okajima K, et al. Reproducibility of geometric distortion in magnetic resonance imaging based on phantom studies. *Radiother Oncol*. 2000;57(2):237–242. doi:10.1016/s0167-8140(00)00234-6.

15   Wang D, Doddrell DM, Cowin G. A novel phantom and method for comprehensive 3-dimensional measurement and correction of geometric distortion in magnetic resonance imaging. *Magn Reson Imaging*. 2004;22(4):529–542. doi:10.1016/j.mri.2004.01.008.

16   Baldwin LN, Wachowicz K, Thomas SD, Rivest R, Fallone BG. Characterization, prediction, and correction of geometric distortion in 3 T MR images. *Med Phys*. 2007;34(2):388–399. doi:10.1118/1.2402331.

17   Baldwin LN, Wachowicz K, Fallone BG. A two-step scheme for distortion rectification of magnetic resonance images. *Med Phys*. 2009;36(9):3917–3926. doi:10.1118/1.3180107.

18   Stanescu T, Jans HS, Wachowicz K, Fallone BG. Investigation of a 3D system distortion correction method for MR images. *J Appl Clin Med Phys*. 2010;11(1):2961. doi:10.1120/jacmp.v11i1.2961.

19   Walker A, Liney G, Metcalfe P, Holloway L. MRI distortion: considerations for MRI based radiotherapy treatment planning. *Australas Phys Eng Sci Med*. 2014;37(1):103–113. doi:10.1007/s13246-014-0252-2.

20   Aoyama T, Shimizu H, Shimizu I, et al. Geometric distortion in magnetic resonance imaging systems assessed using an open-source plugin for scientific image analysis. *Radiol Phys Technol*. 2018;11(4):467–472. doi:10.1007/s12194-018-0477-y.

21   Karger CP, Höss A, Bendl R, Canda V, Schad L. Accuracy of device-specific 2D and 3D image distortion correction algorithms for magnetic resonance imaging of the head provided by a manufacturer. *Phys Med Biol*. 2006;51(12):N253–N261. doi:10.1088/0031-9155/51/12/N04.

22   Fukuyama A, Isoda H, Koyama S. Development of the phantom to measure the image distortion in the magnetic resonance angiography and verification of the relationship between geometric positions and the image distortion. *Proceedings of the 24th Annual Meeting of ISMRM*. Singapore, 2016;2529.

23   Tofts PS. Standing waves in uniform water phantoms. *J Magn Reson B*. 1994;104:143–147. doi:10.1006/jmrb.1994.1067.

24   Pappas EP, Alshanqity M, Moutsatsos A, et al. MRI-related geometric distortions in stereotactic radiotherapy treatment planning: evaluation and dosimetric impact. *Technol Cancer Res Treat*. 2017;16(6):1120–1129. doi:10.1177/1533034617735454.

25   Chang H, Fitzpatrick JM. A technique for accurate magnetic resonance imaging in the presence of field inhomogeneities. *IEEE Trans Med Imaging*. 1992;11(3):319–329. doi:10.1109/42.158935.

26   Kamomae T, Shimizu H, Nakaya T, et al. Three-dimensional printer-generated patient-specific phantom for artificial in vivo dosimetry in radiotherapy quality assurance. *Phys Med*. 2017;44:205–211. doi:10.1016/j.ejmp.2017.10.005.

27   Grodzki DM, Jakob PM, Heismann B. Ultrashort echo time imaging using pointwise encoding time reduction with radial acquisition (PETRA). *Magn Reson Med*. 2012;67:510–518. doi:10.1002/mrm.23017.

28   Ghose S, Rai R, Dowling J, Arumugam S, Schmitt B, Liney G. The potential role of ultrashort echo time sequences in MRI guided radiotherapy. *MReadings: MR in RT*. Siemens;2015:82–85.

29   Nyholm T, Jonsson J. Counterpoint: Opportunities and challenges of a magnetic resonance imaging-only radiotherapy work flow. *Semin Radiat Oncol*. 2014;24:175–180. doi:10.1016/j.semradonc.2014.02.005.